

Development of a Cost-Effective 1.5kN Liquid-Fueled Rocket Propulsion System

Jason Chen ^{*1}, Srikanth Gouru ^{†2}, Sophia Troshynski ^{‡3}, Ron Nachum ^{§4}, Ankit Khandelwal ^{¶5}, Ethan Ai ^{||6}, and Dabini Muldoon ^{**7}

¹Project Lead and Chief Engineer, ²Flight and Ground Software Lead, ³Manufacturing Lead,
⁴Propulsion Lead, ⁵Avionics Lead, ⁶CAD and Testing Lead, ⁷Structures and Ground Operations Lead



Project Caelus, 501(c)(3)
(Initial revision 06 August, 2019; received 26 March, 2020)

This is an example of the abstract. Mit der CNN.com Europe Edition verfügt der TV-Sender CNN über eine umfassende Webseite, die im Minutentakt rund um die Uhr aktualisierte Weltnews aus einer europäischen Perspektive auf den Bildschirm bringt. Wichtige, globale Ereignisse, geordnet in den Rubriken breaking news, current news headlines oder in depth, werden mit Hilfe von Video- und Audioclips, Bildern, Karten, Profilen, Zeitachsen und Tatsachenberichten fundiert dargestellt. Die Nachrichten stützen sich auf die Expertenanalysen der CNN Korrespondenten. Die Berichte verweisen auf andere relevante CNN Reportagen und zu Meldungen anderer Websites. Zusätzlich besteht die Möglichkeit, Videos anzufordern und mittels einer Suchfunktion Zugriff auf bereits gesendete Berichte und gesonderte Themenbereiche, die seit 1995 bearbeitet wurden, zu erhalten.

1 Nomenclature

Symbols	Acronyms
ϵ	= Expansion ratio
γ	= Ratio of specific heats
ρ	= Density
C^*	= Characteristic velocity
C_d	= Discharge coefficient
C_v	= Valve flow coefficient
f_d	= Friction factor
F_t	= Thrust
g_0	= Acceleration due to gravity
I_{sp}	= Specific impulse
\dot{m}	= Mass flow rate
O/F	= Oxidizer-to-fuel ratio
Q	= Volumetric flow rate
	CEA = Chemical equilibrium with applications
	g/cm^3 = Commercial off-the-shelf
	m/s = Data acquisition & control
	FOD = Foreign object debris
	$GLOW$ = Gross lift-off weight
	$MECO$ = Main engine cut-off
	$P&ID$ = Piping and instrumentation diagram
	N = Pressure transducer
	m/s^2 = PT
	s = Thermocouple
	kg/s = SF
	L/s = Safety factor
	VDC = Direct current voltage

^{*}jay.chen135@gmail.com, contact@projectcaelus.org

[†]srikarg89@gmail.com

[‡]stroshynski@gmail.com

[§]ronnachum13@gmail.com

[¶]amtron521@gmail.com

^{||}ethanai22@gmail.com

^{**}cdabinim2249@gmail.com

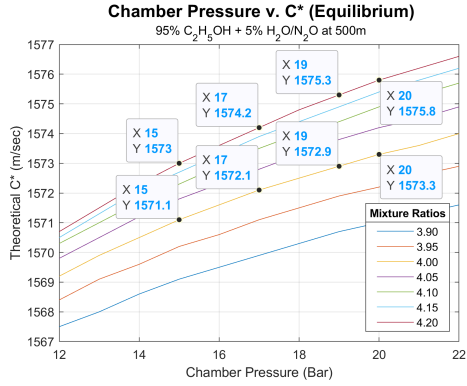


Figure 1: Theoretical C^* efficiency vs chamber pressure and numerous mixture ratios.

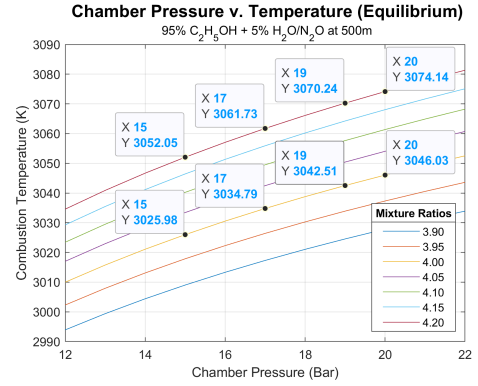


Figure 2: Combustion temperature vs chamber pressure and numerous mixture ratios.

Note: Subscripts follow the convention outlined in [3]. Unless otherwise specified, subscript 0 indicates at stagnation or impact conditions, 1 indicates conditions at the nozzle inlet or combustion chamber, t indicates the nozzle throat, 2 is at the nozzle exit, and 3 is at ambient conditions.

2 Initial System Characterization

Project Caelus's unique position as a 501(c)(3) non-profit organization consisting entirely of high school students has laid the foundation for a design approach fully committed to cost-effectiveness, simplicity, and reliability. The following section outlines the initial design choices made for our overall system and reflects our emphasis on the aforementioned ideals.

2.1 Objectives

The Callisto 1 system is set to the following constraints and objectives:

1. Reach an altitude of 1500 m (\approx 5000 ft).
2. A *GLOW* of no more than 30 kg (\approx 70 lbsm).
3. A nominal main engine thrust of 1.5 kN (\approx 350 lbsf).
4. A chamber pressure in the range of around 15 Bar to 20 Bar (\approx 218 psi to 300 psi)
5. A nominal burn time of around 5 seconds.
6. Consume a budget of no more than \$10,000 USD.
7. Utilize 95% ethyl alcohol and nitrous oxide as the propellant combination.

2.2 Chamber Pressure and Mixture Ratio Selection

The first step is to realize the theoretical maximum performance to be expected from our propellant combination. 95% ethyl alcohol (ethanol) was chosen for its availability, low pricing, and a modest specific impulse. A 95% dilution (by mass) with water was chosen as to lower the expected combustion chamber temperature. This trade-off sacrifices some I_{sp} but reduces engineering complexity as regenerative and film cooling circuits may not be required. Industrial nitrous oxide was chosen as the main oxidizer for its self-pressurizing characteristics, non-cryogenic nature as opposed to liquid oxygen, relative ease to obtain, and a modest I_{sp} with ethanol. Using CEA, an open-source thermodynamics library provided by NASA's Glenn Research Center, critical data describing propellant combustion characteristics could be obtained. Numerical Python scripts were written to iterate through various combustion chamber pressures and mixture ratios and interface with CEA, and MATLAB scripts were used to parse and graph the CEA outputs as shown in Figures 1, 2, 3, and 4. Mixture ratios of 4.0 and 4.2 are labeled at certain chamber pressures. All dependent-variable properties (characteristic velocity C^* , combustion

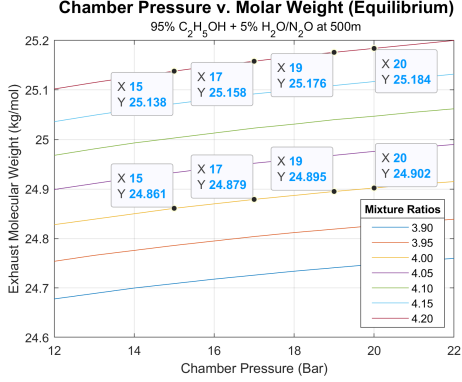


Figure 3: Gas molecular mass vs chamber pressure and numerous mixture ratios.

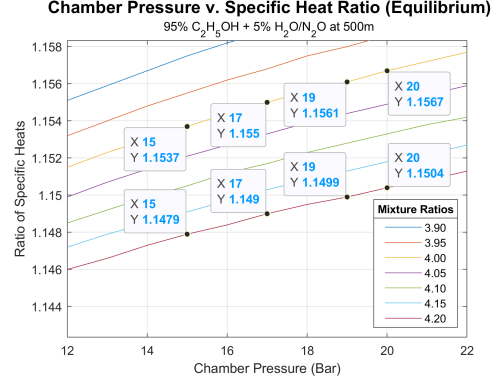


Figure 4: Ratio of specific heats vs chamber pressure and numerous mixture ratios.

temperature T_c , exhaust molar mass M , and exhaust specific heat ratio γ) were permuted assuming shifting equilibrium flow and at an operational altitude of 500 m.

A mixture ratio of 4.0 was chosen for Aphlex 1B mainly in the interest of a conservative combustion temperature of around 3026 K and a middle-of-the-line theoretical C^* of around 1570 m/s, given a chamber pressure of 15 bar. This chamber pressure was chosen primarily in the interest of saving costs. A lower chamber pressure minimizes upstream fluid pressures and thus tank weight requirements, as well as requiring less expensive equipment that may otherwise be required. Although engine efficiency is sacrificed, this was not of primary concern. Preliminary literature reviews additionally showed that 15 bar (≈ 218 psi) was around the minimal operable chamber pressure, since a further decrease in chamber pressure would not allow critical pressure, a requirement for choked flow at the nozzle throat, to occur.

3 Propulsion System Design

The following section outlines the design process for Aphlex 1B, our second-generation bi-propellant liquid rocket engine, set to fly on our 30 kg launch vehicle, Callisto 1, given the objectives and data obtained in the previous section.

3.1 Nozzle Design

Design Parameters and Fluid Characteristics		
Name	Value	Unit
Propellant (Fuel)	Ethanol (C_2H_5OH , 95%)	N/A
Propellant (Oxidizer)	Nitrous oxide (N_2O)	N/A
O/F , Oxidizer/fuel ratio	4.0	N/A
F_t , Nominal thrust	1.50	kN
t_b , Burn time	5.0	sec
I_{total} , Total impulse	7500	N * s
P_c , Chamber static pressure	1.5×10^6	Pa
P_e , Ambient pressure	9.5540×10^4	Pa
T_c , Chamber static temperature	3025.98	K
M , Exhaust molecular mass	24.861	kg/mol
γ , Specific heat ratio	1.1537	N/A

Table 1: Summary of design parameters and fluid characteristics.

$$T_3 = 15.04 - 0.00649h \quad (3.1)$$

$$P_3 = \left[101.29 \times \left(\frac{T + 273.1}{288.08} \right)^{5.256} \right] \times 1000 \quad (3.2)$$

The nozzle design process followed standard procedures outlined in Rocket Propulsion Elements [3] and open-source NASA documents. The thermodynamic properties of the exhaust gas and other important parameters are summarized and compiled in Table 1. The ambient pressure was calculated using NASA Glenn Research Center's Earth Atmosphere Model for an altitude within the troposphere (less than 11000 meters), as shown in Equations 3.1 and 3.2, where T_3 represents the ambient temperature in Kelvin, h is the altitude in meters, P_3 is the ambient pressure in Pascals.

Assuming fully isentropic flow (by definition both adiabatic and reversible) in the supersonic nozzle with choked flow conditions at the throat, an ideal converging-diverging (de Laval) nozzle can be characterized. The first parameter to calculate is the controlling area ratio

$$\frac{A_t}{A_2} = \left(\frac{\gamma + 1}{2} \right)^{1/(\gamma-1)} \left(\frac{p_2}{p_1} \right)^{1/\gamma} \sqrt{\frac{\gamma + 1}{\gamma - 1} \left[1 - \left(\frac{p_2}{p_1} \right)^{(\gamma-1)/\gamma} \right]} \quad (3.3)$$

where A_t is the cross-sectional area of the throat, A_2 is the cross-sectional area at nozzle exit, and p_1 and p_2 are the chamber pressure and exit pressure respectively. Equation 3.3 is also often referred to as the inverse of the expansion ratio ϵ , since $\epsilon = A_2/A_t$. Evaluating Equation 3.3 gives

$$\frac{A_t}{A_2} = \left(\frac{2.15}{2} \right)^{1/0.15} \left(\frac{9.6 \times 10^4}{1.5 \times 10^6} \right)^{1/1.15} \sqrt{\frac{2.15}{0.15} \left[1 - \left(\frac{9.6 \times 10^4}{1.5 \times 10^6} \right)^{0.15/1.15} \right]} = 0.307$$

Notice the substitution of p_2 for P_e as specified in Table 1, since in an ideal nozzle, the exhaust gas should expand to ambient pressure. The expansion ratio ϵ is simply

$$\epsilon = A_2/A_t = 1/AR = 1/0.307 = 3.26$$

Next, we can find the ideal exit velocity v_2 , sometimes denoted as c :

$$v_2 = \sqrt{\frac{2\gamma}{\gamma-1} \left(\frac{R_u T_1}{M} \right) \left[1 - \left(\frac{p_2}{p_1} \right)^{(\gamma-1)/\gamma} \right]} \quad (3.4)$$

where R_u is the universal gas constant of 8314.3 J/kg mol-K and M is the molecular mass of the gas as shown in Table 1. Evaluating gives

$$v_2 = \sqrt{\frac{2 * 1.15}{0.15} \left(\frac{8314.3 * 3026}{24.86} \right) \left[1 - \left(\frac{9.6 \times 10^4}{1.5 \times 10^6} \right)^{0.15/1.15} \right]} = 2162.3 \text{ m/s}$$

Next, the mass flow rate \dot{m} can be calculated explicitly noting that $v_2 = c$, since earlier it was stated that $p_2 = p_3$:

$$\dot{m} = F_t/c = 1500/2162.3 = 0.694 \text{ kg/s} \quad (3.5)$$

Solving using our chosen O/F ratio of 4.0 for each independent propellant \dot{m} gives

$$\begin{aligned} \dot{m}_o &= \dot{m} * (4/5) = 0.694 * (4/5) = 0.555 \text{ kg/s} \\ \dot{m}_f &= \dot{m} * (1/5) = 0.694 * (1/5) = 0.139 \text{ kg/s} \end{aligned}$$

Next, we arrive at the throat area:

$$A_t = \frac{\dot{m}}{p_1} \sqrt{\frac{(R_u/M)T_1}{\gamma[2/(\gamma+1)]^{(\gamma+1)/(\gamma-1)}}} \quad (3.6)$$

Evaluating Equation 3.6 gives

$$A_t = \frac{0.694}{1.5 \times 10^6} \sqrt{\frac{(8314.3/24.86) * 3026}{1.15[2/(2.15)]^{(2.15)/(0.15)}}} = 7.29 \times 10^{-4} \text{ m}^2 = 7.29 \text{ cm}^2$$

Using this calculated throat area and the expansion ratio, the exit area is simply

$$A_2 = \epsilon * A_t = 3.26 * 7.29 \times 10^{-4} = 2.38 \times 10^{-3} \text{ m}^2 = 23.8 \text{ cm}^2 \quad (3.7)$$

From the parameters calculated thus far, we can calculate some useful performance metrics such as I_{sp} and thrust coefficient C_F :

$$(I_{sp})_{opt} = F_t / (\dot{m} * g_0) = c/g_0 = 2162.3/9.81 = 220.42 \text{ sec} \quad (3.8)$$

where g_0 is the acceleration due to gravity at Earth's surface. C_F is

$$(C_F)_{opt} = \frac{F_t}{p_1 A_t} = \frac{1500}{1.5 \times 10^6 * 7.29 \times 10^4} = 1.372 \quad (3.9)$$

Note that under a more rigorous derivation, C_F can be seen to be a key parameter for analysis and varies depending on γ , the nozzle expansion ratio ϵ , and the pressure ratio p_1/p_2 . Normally, C_F is experimentally determined by measuring chamber pressure, throat diameter, and thrust. The optimal C_F and therefore F_t occur when $p_2 = p_3$.

Finally, the physical dimensions of the nozzle can be determined using simple trigonometry via a standard convergence half-angle α of 45° and a standard divergence half-angle β of 15° . The characteristic chamber length L^* , a parameter used for characterizing the necessary chamber volume for adequate mixing and combustion of the propellants, must be more carefully considered. Ideally, L^* is purely a function of the chemistry of the propellant combination and is often based upon previous successful engine designs [3]. However, due to the dynamical and complex nature of nitrous oxide, such as exothermic decomposition after vaporization in the injector and a high density sensitivity to temperature, a more sophisticated model is needed to calculate L^* . Palacz proposes an explicit equation for finding the ideal L^* for a nitrous oxide system, and empirically determined an ideal range for an NO_x /ethanol system of L^* values from 125.6 cm to 167.8 cm [1]. This range is confirmed by Sutton and Biblarz, as L^* values of between 1.0 m and 1.5 m are expected with ethanol systems. A low-range L^* value of 1.25 m was chosen as a smaller form factor is desired over perfect combustion efficiency. L^* is mathematically defined as

$$L^* = \frac{V_c}{A_t} = \frac{\pi r_c^2 L_c}{A_t} \implies L_c = \frac{A_t L^*}{\pi r_c^2} \quad (3.10)$$

where L_c is the length of the chamber and r_c is the radius of the chamber. It is apparent that the a desired form factor can be obtained by adjusting either the radius or the length of the chamber. Through iteration, a chamber radius r_c of 4.0 cm was chosen. The only constraint on the chamber radius is the contraction ratio, defined as A_1/A_t (the ratio of chamber area to throat area), which must achieve a value of 4.0 or more [3]. A trivial area calculation can be performed to confirm that this constraint is satisfied: $CR = \pi r_c^2 / A_t = 5.03 \times 10^{-4} \text{ m}^2 / 7.29 \times 10^{-4} \text{ m}^2 = 6.90 > 4.0$. The chamber length is therefore

$$L_c = \frac{A_t L^*}{\pi r_c^2} = \frac{(7.29 \times 10^{-4} \text{ m}^2)(1.25 \text{ m})}{5.03 \times 10^{-4} \text{ m}^2} = 0.1813 \text{ m} = 18.13 \text{ cm}$$

Calculated Performance Parameters		
Name	Value	Unit
\dot{m} , Total mass flow rate	0.694	kg/s
\dot{m}_f , Fuel mass flow rate	0.555	kg/s
\dot{m}_o , Oxidizer mass flow rate	0.139	kg/s
v_2 , Exhaust velocity	2162.3	m/s
$(I_{sp})_{opt}$, Specific impulse (optimal)	220.42	s
$(C_F)_{opt}$, Thrust coefficient (optimal)	1.372	N/A

Table 2: Summary of engine performance parameters.

Table 2 shows the calculated engine parameters and Table 3 shows the calculated physical nozzle dimensions. Using the data from Table 3, a basic conical nozzle can be realized.

Figure 5 shows the basic conical nozzle for Aphlex 1B created using the given dimensions. Although a conical nozzle may exhibit an advantage in its ease of manufacturing, it is sub-optimal for performance since 1) the exhaust is not exiting the nozzle completely parallel to the nozzle axis, which results in lateral losses of energy, 2) the sharp convex corner at the throat generates shocks which are not adequately dissipated by a conical nozzle, and 3) the small divergence half-angle ensures a long diverging section, which increases engine mass. To address these issues, most modern nozzles are so-called “bell” nozzles, whose diverging section includes a straightening section to address the first issue and inherently addresses

Calculated Dimensional Parameters		
Name	Value	Unit
α , Convergence half-angle	45	deg
β , Divergence half-angle	15	deg
A_t , Throat area	7.29×10^{-4}	m^2
A_2 , Exit area	2.38×10^{-3}	m^2
A_c , Chamber cross-sectional area	5.03×10^{-4}	m^2
R_t , Throat radius	15.23	mm
R_2 , Exit radius	27.52	mm
R_c , Chamber radius	40.0	mm
L_c , Chamber length	181.3	mm
ϵ , Expansion ratio	3.26	N/A
CR , Contraction ratio	6.9	N/A

Table 3: Summary of physical nozzle dimensions.

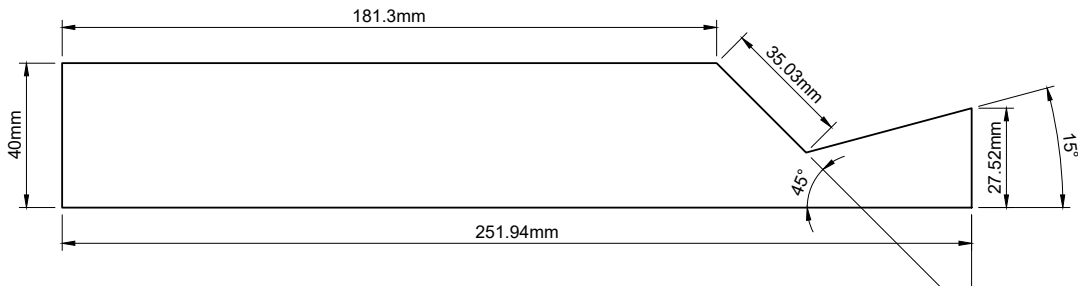


Figure 5: Aphlex 1B drawing with a conical nozzle and given dimensions.

the third issue by having a more rapidly expanding cross-section as compared to conical nozzles. To neutralize the Prandtl-Meyer expansion fans generated at the sharp corner of the throat, a numerical technique called the Method of Characteristics (MOC) is used to generate the nozzle contour.

In brief, MOC propagates characteristic lines emanating from the throat, and by using equations to model characteristic interactions and reflections, it is able to generate a nozzle contour to precisely neutralize (reflect in a manner parallel to the nozzle axis) these expansion fans. A MATLAB script was written to execute and create the MOC nozzle, which can be found on our Project Caelus propulsion GitHub repository at https://github.com/ProjectCaelus/propulsion/blob/master/nozzle-calculations/moc_nozzle.m. Its output is shown in Figure 6. The Cartesian points representing the generated wall contour were exported as a CSV file, which was then imported into our computer-aided design (CAD) program, Fusion 360, where a best-fit nth-order spline was used to finalize the diverging contour. Although the shape of the diverging section can be optimized significantly, the precise shape of the nozzle converging section has not been found to heavily impact engine performance and is therefore smoothed

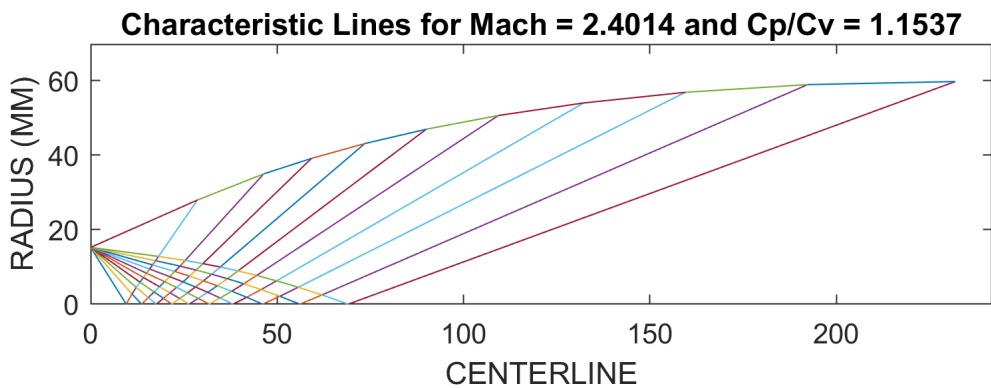


Figure 6: MATLAB visualization for MOC. Shown are the characteristic lines and the generated nozzle contour.

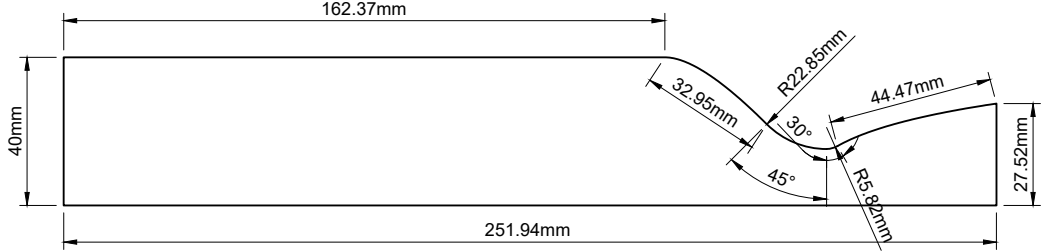


Figure 7: Aphlex 1B drawing with a MOC nozzle and given dimensions.

under the guidelines of Dr. GVR Rao's parabolic approximation method [3][2].

3.2 Injector Design

The injector serves two main purposes in a liquid rocket engine: the adequate mixing (atomization) of the incoming propellant streams to ensure maximum combustion efficiency and the prevention or minimization of combustion instabilities. Some injectors additionally implement film cooling to aid in reducing the thermal load of the chamber and nozzle walls, however, our system relies solely on the heat capacity of the chamber walls and a thin ablative layer to maintain wall integrity. This is done since it would save propellant mass that would otherwise be wasted for film cooling and due to the relatively short burn time of our system.

3.2.1 Selection of Element Type

There are many types of injector elements, each with unique advantages and disadvantages. The injector types considered were the triplet (fuel-centered) unlike impinging injector and the like-on-like doublet impinging injector, due to 1) our limited manufacturing capabilities 2) a fairly unbalanced O/F ratio 3) both types exhibiting good mixing and atomization properties and 4) the abundance of historical experience and data with both injector types. Both the coaxial swirl and pintle types were deemed either too complex to manufacture or too difficult to characterize due to a limited amount of available documentation. NASA's SP-8089 conference document on liquid engine injector design suggests that the best way to characterize both the individual orifice geometries and the overall injector geometry for unlike impinging injectors is through diameter ratios. Vigorous cold flow and other empirically testing methods at the time were used and have found correlations between the driving orifice diameter ratio with the optimum mixing efficiency. The correlation found was

$$\left(\frac{d_c}{d_{ou}}\right)^2 = M \left[\frac{\rho_{ou}}{\rho_c} \left(\frac{\dot{m}_c}{\dot{m}_{ou}} \right)^2 \right]^{0.7} \quad (3.11)$$

where d_c is the diameter of center orifice, d_{ou} is the diameter of an outside individual orifice, M is an experimentally-determined mixing factor coefficient, ρ represents liquid density, and \dot{m}_c and \dot{m}_{ou} are the center mass flow rate and outside mass flow rate respectively. It is cited that for a 2-on-1 element type, M has a value of 1.6. Using Equation 3.11, we find that our controlling diameter ratio is

$$\frac{d_c}{d_{ou}} = \sqrt{M \left[\frac{\rho_{ou}}{\rho_c} \left(\frac{\dot{m}_c}{\dot{m}_{ou}} \right)^2 \right]^{0.7}} = \sqrt{1.6 \left[\frac{772.25 \text{ kg/m}^3}{789 \text{ kg/m}^3} \left(\frac{0.1389 \text{ kg/s}}{0.5556 \text{ kg/s}} \right)^2 \right]^{0.7}} = 0.4757$$

Since this diameter ratio is not reasonably near 1.22 (as suggested by NASA SP-8089), we can assume this correlation would not be accurate and that there will be potentially drastic losses in mixing efficiency. Thus, this suggests that a like-on-like system is required.

3.2.2 Main Injector Parameterization

Since like-on-like elements will have a 1 to 1 diameter and momentum ratio, we can begin determining the pressure drop and mass flow rate through each individual orifice. Rocket Propulsion Elements (RPE)

provides an equation for the volumetric flow rate Q (and therefore \dot{m} since ρ is constant) as shown below:

$$\dot{m} = Q\rho = C_d A \sqrt{2\rho\Delta p} \implies \Delta p = \left[\left(\frac{\dot{m}}{C_d A} \right)^2 \right] / 2\rho \quad (3.12)$$

where C_d is a dimensionless discharge coefficient that is experimentally determined and a function of the orifice geometry, A is the area of the orifice, and Δp is the pressure drop across the orifice. Flow velocity is similar:

$$v = Q/A = C_d \sqrt{2\Delta p/\rho} \quad (3.13)$$

Since C_d is a measured parameter, initial design calculations must assume a value. RPE suggests a C_d value of around 0.88 for a 1 mm diameter orifice in a short tube with a rounded entrance (assuming an orifice length to diameter ratio of $L/D > 3.0$), and 0.9 for a similar configuration with a 1.57 mm diameter. Accordingly, a C_d value of 0.9 was chosen for the oxidizer and a C_d value of 0.88 was chosen for the fuel. For the orifice sizing, NASA SP-8089 found that smaller orifice sizes attributed to better mixing in all scenarios, although only to a certain extent (orifice diameters < 0.03 inches saw insignificant improvements in mixing). Due to limited manufacturing capabilities, a minimum hole size of 1 mm was chosen. Using this information, a design parameter of an overall injector pressure drop that is 25% of chamber pressure, and Equation 3.12, the mass flow rate across a single oxidizer and fuel orifice are

$$\dot{m}_o = 0.9 * (\pi * ((1.58 \text{ mm}/2) \times 10^{-3})^2) \sqrt{2(772.25 \text{ kg}/\text{m}^3)(1.5 \times 10^6 \text{ Pa} * 0.25)} = 0.0425 \text{ kg/s}$$

$$\dot{m}_f = 0.88 * (\pi * ((1.00 \text{ mm}/2) \times 10^{-3})^2) \sqrt{2(789 \text{ kg}/\text{m}^3)(1.5 \times 10^6 \text{ Pa} * 0.25)} = 0.0168 \text{ kg/s}$$

The same pressure drops can be used for each orifice due to Bernoulli's principle and the law of conservation of energy, similar to how voltage stays constant across a parallel circuit. The corresponding injection velocities (Equation 3.13) are

$$v_o = 0.9 \sqrt{(2(1.5 \times 10^6 \text{ Pa})(0.25)) / (772.25 \text{ kg}/\text{m}^3)} = 28.048 \text{ m/s}$$

$$v_f = 0.88 \sqrt{(2(1.5 \times 10^6 \text{ Pa})(0.25)) / (789 \text{ kg}/\text{m}^3)} = 27.132 \text{ m/s}$$

Dividing the mass flow rate by the individual orifice mass flow rates gives the total orifice count for each propellant, denoted as n_o and n_f :

$$n_o = \dot{m}_o / \dot{m}_{oi} = (0.4865 \text{ kg/s}) / (0.0425 \text{ kg/s}) = 11.447$$

$$n_f = \dot{m}_f / \dot{m}_{fi} = (0.139 \text{ kg/s}) / (0.0168 \text{ kg/s}) = 8.27$$

Since both an integer and even amount of holes are obviously required for a like-on-like impinging injector, Equation 3.12 is rearranged to compute the necessary diameter given the desired number of orifices, given a reasonable range of orifice count provided by the previous calculation:

$$d = 2 \sqrt{\frac{\dot{m}}{C_d n \pi \sqrt{2\rho\Delta p}}} \quad (3.14)$$

Solving Equation 3.14 for both oxidizer and fuel streams yields

$$d_o = 2 \sqrt{\frac{0.555 \text{ kg/s}}{(0.9)(16)\pi \sqrt{2(772.25 \text{ kg}/\text{m}^3)(1.5 \times 10^6 \text{ Pa})(0.25)}}} = 0.001428 \text{ m} = 1.43 \text{ mm}$$

$$d_f = 2 \sqrt{\frac{0.139 \text{ kg/s}}{(0.88)(8)\pi \sqrt{2(789 \text{ kg}/\text{m}^3)(1.5 \times 10^6 \text{ Pa})(0.25)}}} = 0.001017 \text{ m} = 1.02 \text{ mm}$$

Thus, to achieve 16 oxidizer orifices and 8 fuel orifices, an oxidizer orifice diameter of 1.43 mm and fuel orifice diameter of 1.02 mm are needed.

The remaining injector parameters were chosen due to a literature review, rather than explicit calculations. The angle of impingement, also known as the cant angle λ , is defined as the angle between two propellant jets. It was chosen to be 60 degrees since it is the most common impingement angle, prevents significant backsplash of propellants onto the injector face (which would produce high heat fluxes with unlike elements), and produces the best atomization characteristics despite requiring a larger L^* .

NASA SP-8089 further suggests that the free-stream jet length (impingement length), defined as the distance from an element face to the point of impingement, should be somewhere in the range of five to seven times the orifice diameter. In other words, $5 < L/D < 7$. An L/D ratio of 6 was chosen, and the free-stream jet length is therefore $(L_{jet})_o = 6 * 1.43 \text{ mm} = 8.57 \text{ mm}$ and $(L_{jet})_f = 6 * 1.02 \text{ mm} = 6.10 \text{ mm}$. The point of impingement (distance of impingement orthogonally measured from the injector face) is therefore $(L_{POI})_o = 8.57 \cos(30) = 7.42 \text{ mm}$ and $(L_{POI})_f = 6.10 \cos(30) = 5.28 \text{ mm}$ since the λ half-angle is 30 degrees.

The thickness of the injector plate is driven by the L/D ratio of the largest orifice (not the jet), which was suggested to be around 10 to ensure smooth and developed flow, assuming the C_d that was used in previous calculations [3]. Simply, $L_{inj} = 10(d_{max}) \cos(\lambda/2)$, since the cosine of the cant half-angle is the coaxial component (thickness). However, a coefficient value of 7 was chosen instead of 10 in the interest of a thinner injector plate. Evaluating gives $L_{inj} = (7)(1.42 \text{ mm}) \cos(30) = 8.608 \text{ mm}$. Finally, finding the distance between each orifice within an element pair involves two separate calculations: one for the distance on the side of the injector face (denoted as “combustor-side”) and one for the distance on its reverse side (denoted as “manifold-side”). First, the combustor-side distance is $d_{com} = (2)(L_{jet}) \sin(30)$, and therefore, $(d_{com})_o = (2)(8.57 \text{ mm}) \sin(30) = 8.57 \text{ mm}$ and $(d_{com})_f = (2)(6.10 \text{ mm}) \sin(30) = 6.10 \text{ mm}$. The manifold-side distance is a case of similar triangles with corresponding combustor-side distances: $(d_{man})_o = [(d_{com})_o / (L_{POI})_o](L_{inj} + (L_{POI})_o) = [8.57 \text{ mm} / 7.42 \text{ mm}](8.61 \text{ mm} + 7.42 \text{ mm}) = 18.512 \text{ mm}$. Similarly, by substituting for fuel parameters: $(d_{man})_f = [6.10 \text{ mm} / 5.28 \text{ mm}](8.61 \text{ mm} + 5.28 \text{ mm}) = 16.045 \text{ mm}$. The final injector parameters are summarized in the table below.

Injector Parameters		
Name	Oxidizer (N_2O)	Fuel (C_2H_5OH)
Injector element type	Doublet like-on-like impingement	
ρ , Density at 298 K	772.25 kg/m^3	789 kg/m^3
\dot{m} , Mass flow rate	0.5552 kg/s	0.1388 kg/s
C_d , Discharge coefficient	0.90	0.88
n , Number of orifices	16	8
d , Orifice diameter	1.43 mm	1.02 mm
A , Individual orifice area	$1.61 \times 10^{-6} \text{ m}^2$	$3.27 \times 10^{-6} \text{ m}^2$
Mass flow rate per orifice	0.0347 kg/s	0.01735 kg/s
λ , Angle of impingement	60°	60°
L_{jet} , Free-stream jet length	8.57 mm	6.10 mm
L_{POI} , Point of impingement	7.42 mm	5.28 mm
Length of orifice	10.00 mm	7.11 mm
d_{com} , Distance between orifices (combustor)	8.57 mm	6.10 mm
d_{man} , Distance between orifices (manifold)	18.51 mm	16.05 mm
L_{inj} , Injector plate thickness	8.608 mm	

Table 4: Summary of injector parameters.

3.2.3 Injector Configuration and Assembly Design

The physical configuration of the injector (element pattern) was chosen largely off common practices and previous injector designs. A standard two-ring pattern was implemented, with the outer ring consisting of the four fuel elements and the inner ring consisting of the eight oxidizer elements. The fuel elements were chosen to reside in the outer ring as to reduce the thermal load on the chamber walls, since it would create a fuel-rich region within the combustion volume. No baffles or other dampening devices were utilized since the chamber is of a small enough volume and the burn time is of short enough duration to neglect most instabilities.

For the injector assembly, two designs were considered: Design A and Design B. Design A features two external common bolts that fasten all injector components together (including the chamber wall), making the assembly modular and consisting of smaller parts. Design B requires more material and has a larger vertical profile than Design A, but is also more streamlined, less complex, contains fewer parts, and requires less machining. Design B was heavily inspired from Michigan Aeronautical Science Association (MASA)’s previous injector designs and is therefore also more proven.

Both designs share a design for the component responsible for the separation of the fuel and oxidizer manifolds. Though Design A is more modular and contains smaller parts, Design B was ultimately

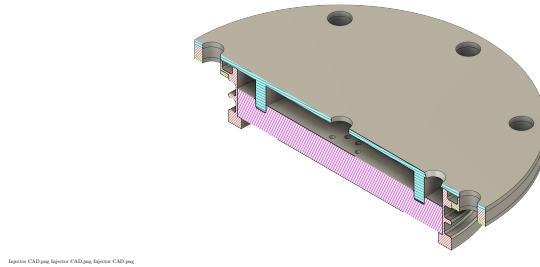


Figure 8: Isometric view of Design A.

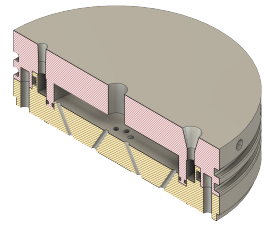


Figure 9: Isometric view of Design B.



Figure 10: Top exploded view of Design B.



Figure 11: Bottom exploded view of Design B.

chosen since it required less manufacturing turn-around, contains only two parts, and unlike Design A, does not unnecessarily widen the engine cross-section.

Orthogonal and cross-sectional views of Design B (which will henceforth be referred to as simply the “injector assembly”) can be seen in Figures 12 and 13. A detailed breakdown of the design is shown in Figure 14 and will be elaborated upon here: the injector assembly comprises of two parts. The manifold plate (1) primarily houses the connection between the main propellant lines and the injector plate. The entirety of the assembly rests within the aluminium walls of the chamber, with the outer face of the manifold plate housing two o-rings that form a seal between the combustion chamber and ambient pressure (OR-2 and OR-3). 14 radial bolts fasten the injector assembly to the chamber wall and also provide the compression necessary for OR-2 and OR-3 to effectively seal. The main oxidizer inlet is located in the center of the manifold plate and allows the oxidizer to transition into the oxidizer manifold (seen as the central scaffolding). The fuel inlet serves a similar purpose but required a lofted entry due to the narrow fuel manifold. Both inlets have an entrance diameter of 1/4”. The fuel and oxidizer manifolds are divided by a separation ring and are sealed by the separator o-rings (OR-4 and OR-5). PT-9 and PT-10, as the name suggests, are 1/8” ports that allow pressure transducers to access to both manifolds. The injector plate (2) houses the propellant orifices and is in direct contact with the combustion chamber. It was designed deliberately to be as simple as possible so that if the relative difficulty in machining the angled orifices causes a manufacturing error, only the plate itself would need to be discarded and re-machined. Although direct contact with the combustion gases may cause significant heating, the high mass flux of propellant in the propellant manifolds effectively cools the injector plate. Eight axial bolts (with bolt heads perturbing into the combustion chamber) fasten the injector plate to the manifold plate. An interface o-ring (OR-1) seals the connection between the fuel manifold and the combustion chamber. A small groove in the bottom left (or right) of the injector plate is to assist in securing the ablative in place.

The next step in the design of the injector assembly was to verify its flow characteristics, such as flow rates, pressures at certain points, and injection velocities. More accurate estimations for such characteristics would allow for comparisons between expected values and those measured during cold flow tests, and therefore test the integrity of our models. Since the use of explicit fluid flow equations to predict flow characteristics heavily impacted by complex geometries is impractical, a numerical approach through computational fluid dynamics (CFD) was used.

The CFD software used was ANSYS Fluent, which includes a streamlined workflow by providing an integrated geometry editor (SpaceClaim), mesher (ANSYS Mesher), solver (Fluent), and post-processor (CFD-Post). This allowed for a quick verification cycle and even parameterized CFD runs. The injector geometry and fluid domain were created in Fusion 360 and imported into SpaceClaim, where parts and boundaries were labeled for the mesher. The mesh was tetrahedron-based and was discretized to around 197,000 elements. In Fluent, the injector material was set to aluminium and the fluid properties were

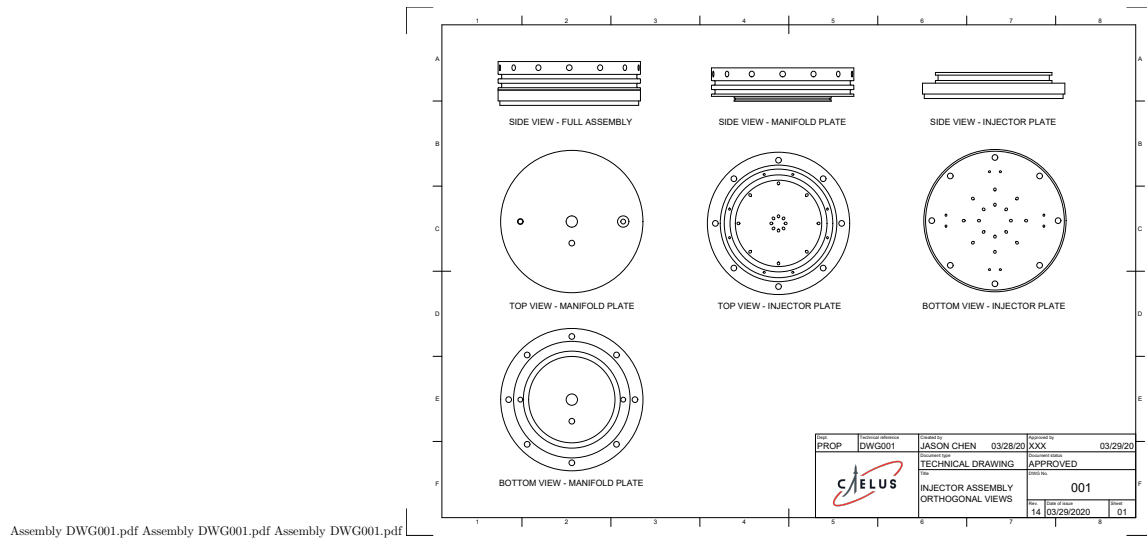


Figure 12: Injector assembly technical drawing orthogonal views.

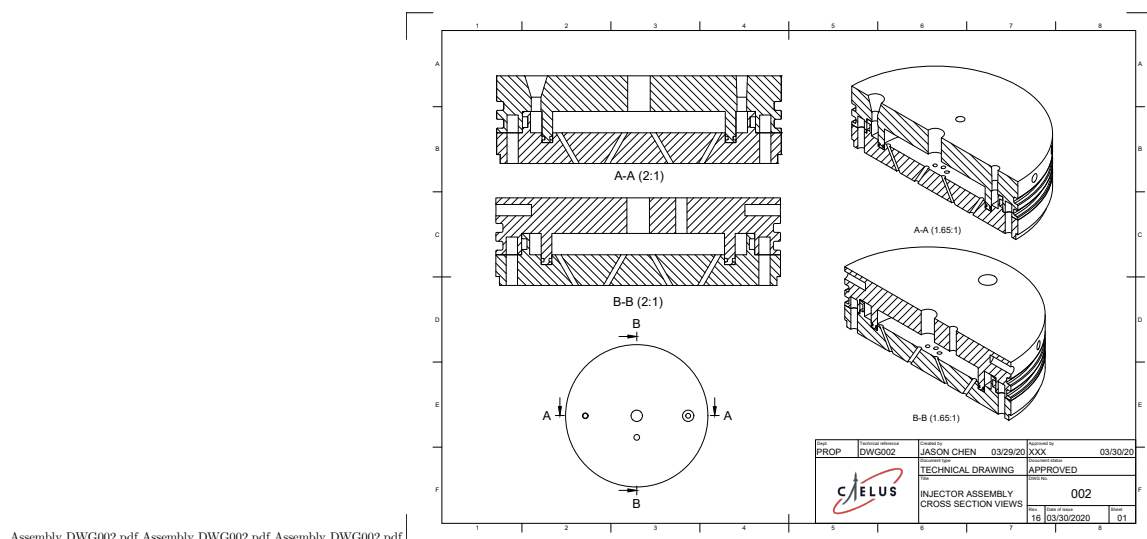


Figure 13: Injector assembly technical drawing cross section views.

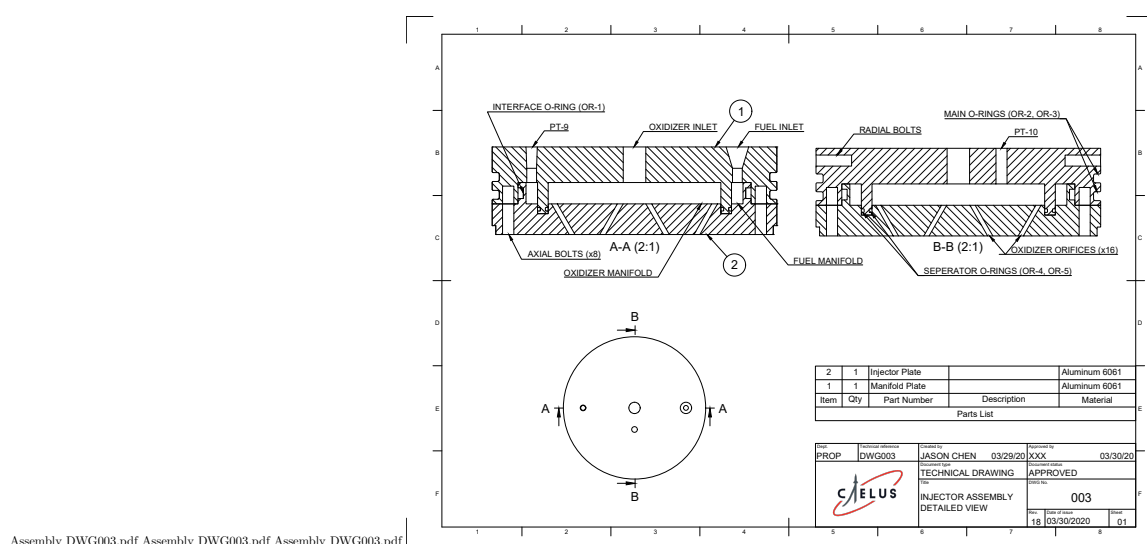


Figure 14: Injector assembly technical drawing detailed description.

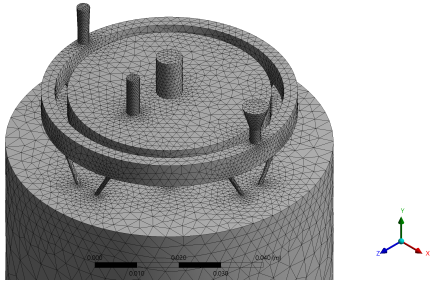


Figure 15: The generated mesh in ANSYS Mesher with $\approx 197,000$ tetrahedron elements.

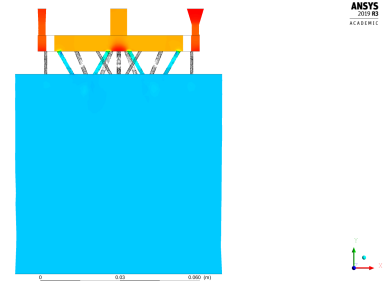


Figure 16: Pressure cross-section contour of the injector assembly and fluid domain.

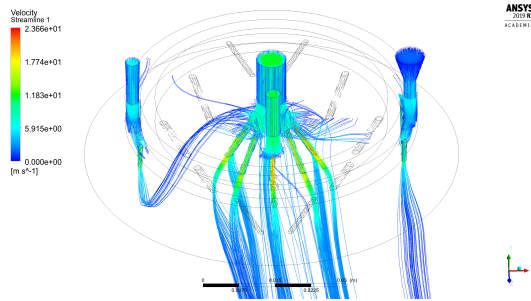


Figure 17: Contoured velocity streamlines (≈ 2500 streamlines). Note the difference in color between the fuel inlet and PT-9, indicating a reduction in pressure.

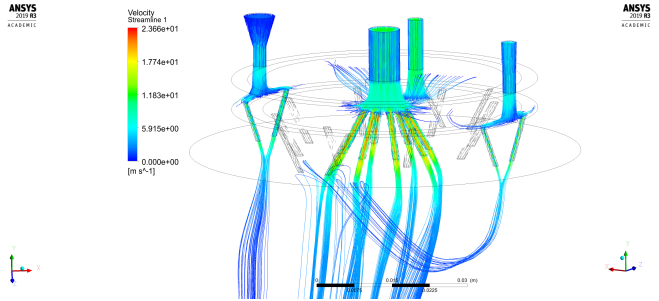


Figure 18: Another view of the contoured velocity streamlines. Note the post-impingement mixing of the outer fuel elements with the inner oxidizer elements.

set to that of ethanol and nitrous oxide at room temperature densities. For the simulation environment, NASA SP-8089 (pp. 35) recommends a pressure drop across the injector between around 15% and 25% of the designated chamber pressure to ensure a steady chamber pressure and prevent feed-coupled instabilities. A liberal Δp of 25% (of P_c) was chosen for this simulation run, i.e. an injector inlet pressure of 1.875×10^6 Pa and outlet pressure (P_c) of 1.50×10^6 Pa was chosen. A more detailed reasoning and explanation for system Δp 's is provided in a later section. A steady-state, pressure-based, k-epsilon viscosity model was used for the solver and ran for 1000 iterations. The results were exported into CFD-Post, where volume and cross-section renderings could be made to analyze the results. Report and data files were also generated. Although other many flow characteristics such as turbulence kinetic energy, temperature, and Reynolds Number could be extracted from the results, static pressure and velocity were the most important parameters and are shown in the post-processing rendering.

Figure 16 and its corresponding output files show that the expected Δp from the propellant piping to the manifold is around 75 kPa (around 20% of the total Δp), while majority of the Δp takes place through the orifices, which is expected. It is also notable that the fuel manifold exhibits a significantly shallower Δp than the oxidizer manifold. This is also expected since the fuel manifold has a significantly smaller volume than the oxidizer manifold. Figure 16 displays a cross section that only shows the impingement of the oxidizer elements. Since the pressure profile for the fuel elements is nearly identical but on a different axis, its contour is not shown here.

Figures 17 and 18 show streamlines (contoured to velocity) of the flow through the injector, with a wireframe of the injector geometry superimposed. Some streamlines were removed in the interest of visibility and to reduce clutter. Figures 19 and 20 show two velocity contours, one of the oxidizer orifices and one of the fuel orifices. Note how the velocity is greatly increased for the oxidizer orifices near the oxidizer inlet in Figure 19. This is to an advantage in terms of mixing efficiency since it would result in a momentum ratio skewed towards towards the chamber walls, which is where the fuel elements reside, thereby mixing the atomized oxidizer droplets with fuel droplets almost immediately. The velocity traces from fuel impingement can also be seen immediately to the left and right of the oxidizer jets. In Figure 20, the velocity contour for a single fuel element is shown. Both figures indicate that an injection velocity of around 15 m/s can be expected.

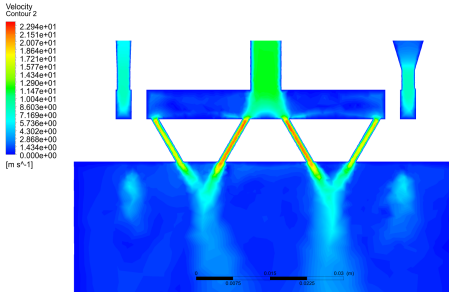


Figure 19: Velocity cross-section contour of the propellant inlets and the oxidizer orifices.

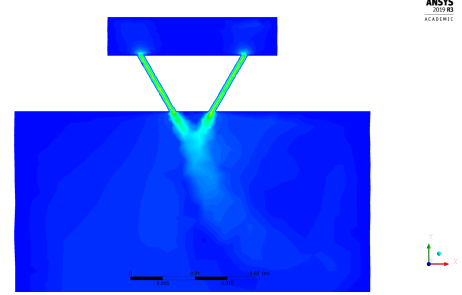


Figure 20: Velocity cross-section contour of fuel orifices. Note the smaller impingement distance.

3.3 Material Selection, Manufacturing, Load and Thermal Analysis

The final step in the design of the injector, thrust chamber, and nozzle is the selection of materials necessary to fabricate these devices, its means of manufacturing, and how these methods are justified through load and thermal analyses.

3.3.1 Material Selection

Three metals were considered as the primary material for the engine system: aluminium, mild steel, and stainless steel. Mild steel could not be used in areas of combustion or areas in contact with nitrous due to its tendency to react with oxidizers. Stainless steel is more expensive, more difficult to machine, and has a lower specific heat capacity and strength-to-weight ratio than aluminium. For these reasons, aluminium (more specifically, 6061 Aluminium) was chosen as the primary material for the injector assembly, the outermost (structural) wall of the combustion chamber, and the nozzle extension. However, one implication of using aluminium is its incompatibility with threads due to its soft nature. Therefore, as seen in Figure 9, female NPT thread ports will need to be welded onto the top face of the manifold to connect the upstream propellant lines to the injector, and threaded inserts will need to be used to accommodate the radial bolt holes that fasten the combustion chamber wall to the injector assembly.

As mentioned in previous sections, the combustion chamber will rely on an ablative layer, held in place by an outer aluminium structural wall, to dissipate heat generated during combustion. There are many candidates for this ablative material, however, under the recommendation of MASA and in the interest of costs and simplicity, a phenolic resin ablative, which is a mix of epoxy and wood/fibrous products, became a prime candidate. PVC has also been shown to be an effective and cheap ablative. However, at this time, the material of the chamber ablative has not been finalized. Interestingly, Copenhagen Suborbitals, an extremely successful amateur rocketry organization based in Denmark, has published their findings in mixing tetraethoxysilane (TEOS) with their ethanol solution as an alternative to fixed ablatives. During combustion, TOES decomposes and leaves a thin layer of silicone dioxide (SiO_2) within the chamber walls, acting as a make-shift ablative. All options will be finalized at a later date.

The converging nozzle and especially the throat, which is the site of highest heat flux in the nozzle and combustion chamber, will be shaped out of graphite. Graphite is one of the best and cheapest ablative materials for heat dissipation due to its molecular structure, and has even been used on large-scale launch vehicles. The primary disadvantage of graphite is that large stocks of the material become exponentially more expensive; this is why graphite was not used as the chamber ablative. Since it is expected that the throat ablative will erode most rapidly, perhaps only being useful for one or two engine burns, the entire engine assembly has been made modular as to easily remove and replace the throat when needed. The diverging nozzle section has a significant impact on performance through its geometry and experiences the least heat flux. Therefore, this nozzle section will be fabricated using aluminum.

Another selection process involved choosing an o-ring material. Briefly, o-rings are seals that prevent fluid flow between two (usually) metallic plates. They work by absorbing heat and responding to the released pressure by expanding to fill the groove. Through several references, primarily Parker's O-Ring Handbook, it was found that the material Perfluoroelastomer (FFKM) is well-suited for the injector assembly based on its high heat tolerance (320 °C, or 593 K) and compatibility with ethanol and nitrous oxide. A specific type of FFKM, FF352, was chosen due to its improved compatibility with nitrous oxide. It was also decided to use a face seal gland since softer edges are required to prevent o-ring damage, and

face seal glands are often utilized when a straight groove is drilled into a flat piece of metal. However, since face seal glands are usually only used at lower temperatures, it is recommended to increase the groove width by some amount to allow for proper expansion of the o-ring in the event that it is exposed to combustion gases.

Parker's O-Ring Handbook also provided guidelines for handling and assembling o-rings. It was mentioned that when assembling the o-ring, stretching it more than 20% of its original length and pinching/twisting the o-ring in any way should be avoided. It is also recommended to lubricate the o-ring with silicone grease or other o-ring greases to prevent a spiral failure (when the o-ring is twisted).

3.3.2 Manufacturing Capabilities and Methods

Due to our budget and circumstances, we do not have direct access to any machine shops or manufacturing facilities. We expect the bulk of our manufacturing needs to be met by local services. This further reiterates the emphasis on simple and cost-effective designs since more complex designs will take more time to manufacture, thus bringing costs up. The only resources we expect to require, however, are a 5-axis CNC mill (for the injector assembly), a laythe (for the combustion chamber and nozzle), and welding materials.

3.3.3 Load and Thermal Analysis

Although thorough load and thermal analyses can be calculated and simulated precisely, in the scope of Aphlex 1B, it is of secondary priority. Preliminary material stress and load simulations were done in ANSYS APDL and Fusion 360's built-in simulation protocol and verified the structural integrity of the injector assembly, but were not extensive. To remedy this, care was taken to ensure material thicknesses were adequate to withstand stresses, and fasteners are added liberally to ensure a robust assembly. The primary material thickness (such as on the chamber wall and nozzle wall) was 2.0 mm, which is more than adequate considering the tensile strength of aluminium. It can loosely be verified by the wall thickness equation provided by [4]:

$$t_{wall} = \frac{P_c r_c}{2\sigma_c} \quad (3.15)$$

where σ_c is the stress on the chamber walls. As for thermal loads, the short burn time of between 3 and 7 seconds is adequate enough to prevent significant overheating. The use of ablatives further widened the safety margin.

Extraneous Injector Parameters		
Name	Value	Unit
Δp_{inj} , Pressure drop across injector, relative to P_c	20	%
$(v_{inj})_e$, Injection velocity (expected)	15	m/s
t_{wall} , Wall thickness	2.0	mm
Injector assembly material	Aluminium 6061	N/A
Combustion chamber structural wall material	Aluminium 6061	N/A
Ablative material	Not yet determined	N/A
Diverging nozzle material	Aluminium 6061	N/A
Converging nozzle and throat material	Graphite	N/A
O-ring material	FFKM (FF352)	N/A

Table 5: Extraneous injector parameters.

4 Plumbing System Design

The design of the plumbing system, the system responsible for carrying the propellant from the propellant tanks to the engine, is a process that is heavily intertwined with ground operations, software design, safety procedures, and the engine design. Due to the complexity of the design process, this section will be partitioned into two sections: a general system design, such as how pressure drops affect tank requirements, piping sizing, and selecting valve trades, and operational design, such as specific filling, pressurization, and safety procedures.

4.1 General System Design

The first step in designing a liquid rocket engine plumbing system involves finalizing the engine cycle. The engine cycle describes the method in which pressurization can be achieved such that the propellants flow follow a positive pressure gradient out of the tanks and into the engine. This may include the use of turbopumps (whether this be driven electrically or with a pre-burner), expander cycles (which use a heat exchanger at the combustion chamber and nozzle to further pressurize the propellant lines), combustion tap-offs, inert gases, or a myriad of other methods. Upholding the philosophy of cost-effectiveness and simplicity, the pressurization of the propellant tanks via an inert gas was chosen (also referred to as a pressure-fed cycle). It requires the least amount of parts and is by far the simplest option.

There are two basic options with a pressure-fed cycle: regulated or unregulated. In a regulated design, there is a separate pressure vessel containing the pressurizing gas, which flows through a regulator and into the main propellant tanks. This regulator serves to maintain a constant pressure even as the propellant in the tanks are expended. In an unregulated design, also known as a blowdown design, the pressurant is stored inside the main propellant tank along with the liquid propellant. This has the obvious disadvantage of exhibiting a dynamic and decaying chamber pressure. A blowdown design was nevertheless selected for its simplicity. It should be noted that only the ethanol tank would require a pressurant and blowdown system, since the nitrous tank is self-pressurizing.

The pressurant gas selection was a straightforward tradeoff. Typically, the pressurizing gas is an inert gas (one that does not react with the liquid propellant it is pressurizing), which leaves essentially two options for the designer: helium or nitrogen. Any gases further down the periodic table are deemed too heavy with no significant advantage. Though helium lighter and is often used with liquid oxygen (LOX) systems since nitrogen dissolves in LOX, it is significantly more expensive. For these reasons, nitrogen was chosen as the pressurant.

With the engine cycle and pressurant determined, a general plumbing system design can be realized. A piping and instrumentation diagram (P&ID) is an overarching flow diagram that details the interactions and connections of parts throughout the entire plumbing system. P&IDs are the standard for representing rocket propulsion plumbing systems and therefore, much care was taken in its conception. All parts of the P&ID have been carefully examined and optimized to fit the mission needs.

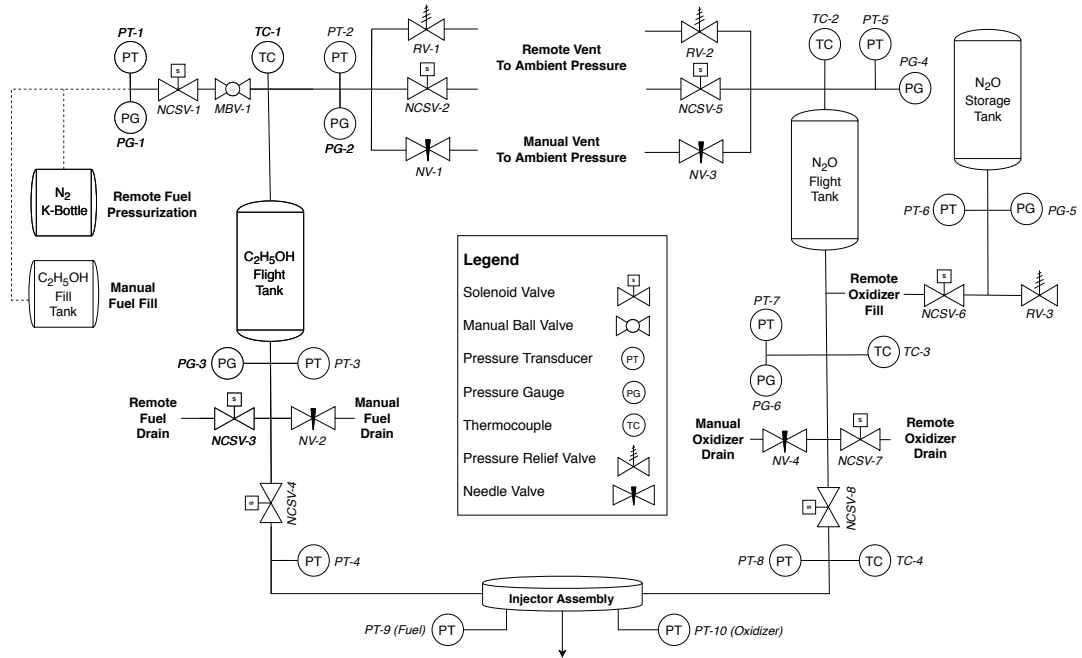


Figure 21: Full system piping and instrumentation diagram (P&ID).

The mechanical and procedural aspects of the P&ID, such as reasoning for fill system procedures and valve types, will be discussed in a later section. Here, attention should be drawn to the general design aspects of the P&ID. First, note the symmetry between both propellant towers. Only the fill and pressurization systems differ. The fill and pressurization systems (ethanol) directly empty into the flight

tank, which indicates the blowdown design. The nitrous flight tank is simply filled by gravity via the nitrous storage tank. During both fill and flight conditions for both towers, a remote and ambient vent of the pressurant is available. Pressure is measured here to monitor tank pressurization and depletion profiles. A thermocouple is also placed here, but is only really necessary on the nitrous tower due to its density and boil rate sensitivity to temperature. Only one valve lies between the flight tank and the injector: the main propellant valve (MPV). The MPV is responsible for simply opening or closing propellant flow to the engine. The MPV is a solenoid valve since proportional control via a ball valve was deemed unnecessary; there is no intention for engine throttling and concerns for a hard start in startup transients can be addressed with a properly designed ignitor and robust flight software. Instruments are placed on either side of the MPV to measure pressure losses, and therefore its C_v . A pair of remote and manual drain valves was placed before the MPV to divert propellants away from the engine in case of an MPV failure or system over-pressurization that cannot be addressed solely by the vent system. No purge lines were implemented since residual propellants inside the propellant lines are not a significant safety concern (neither propellants are particularly toxic or cryogenic).

With a P&ID drafted, the next step becomes to determine the physical characteristics of the plumbing system, such as tank dimensions, pipe diameters, valve trades, and flow characteristics.

4.2 System Pressure Drop Δp_{sys}

The first and most important step to conceptualizing the physical characteristics of the plumbing system is to determine the required tank volumes and pressures. The tank pressure and pressure profile drives every component downstream of it, which is effectively the entire system. But to achieve this, it is necessary to first determine the pressure drops expected throughout the plumbing system so that a minimum final tank pressure can be set. This is done as to prevent blowback from the combustion chamber near the end of an engine burn and represents the expected final system state. Characterizing the expected pressures at different points within the system is also useful as expected values when comparing to empirical data. This total sum of pressure drops between the propellant tank and combustion chamber, Δp_{sys} , can be decomposed into individual part losses (flow barriers such as valves), frictional losses through the raw length of the pipe (head loss and other effects), and the injector Δp . Mathematically:

$$\Delta p_{sys} = \Delta p_{inj} + \Delta p_{val} + \Delta p_{ext} \quad (4.1)$$

The previous section has already established that Δp_{inj} obtains a value of 20% P_c , which evaluates to $\Delta p_{inj} = 300 \text{ kPa}$. The remaining two terms will be elaborated upon further in the following subsections.

4.2.1 Pipe Length and Extraneous Pressure Losses Δp_{ext}

¹

Modelling compressible viscous flow through a pipe is a nontrivial task. To avoid lengthy theoretical calculations that would otherwise be overshadowed by empirical data anyway, assumptions were made about the fluid flow to simplify the pipe sizing and pressure loss calculations. The two most important of these assumptions are that 1) there are no swirl, entrance, or heat-transfer effects, and 2) the pipe is completely circular. A short derivation for the necessary equations for calculating Δp_{ext} starts simply with the classic case of Bernoulli's Equation:

$$p + \frac{1}{2}\rho V^2 + \rho g_0 z = \text{constant} \quad (4.2)$$

It gives insight into the balance between pressure, velocity, and elevation by assuming that the two points in question lie on a streamline, the fluid is incompressible, the flow is steady and inviscid, and there is no friction. Although useful for some applications, it is not adequate for designing robust piping systems which will in actuality encounter such effects.

The addition of a *head loss* term, denoted as h_f , is important in introducing a viscous term in an otherwise inviscid equation. Head loss can simply be thought of as an additional pressure loss in the system due to viscous effects, a sudden expansion/contraction, and/or obstructions to its path such as pipe elbows, bends, valves, etc. To introduce the head loss term into a useful form for solving pipe flow

¹In the following subsection, some explanatory tools, such as derivations and figures, are heavily inspired from the work of [5]. Any figures extracted from [5] are strictly

for the purpose of visualization, explanation, and education. We make no claims and have no intention in claiming ownership or rights to these graphics.

problems, there is the famous *Darcy-Weisbach equation*, which is a proposed correlation valid for duct flow of any cross section and any Reynolds Number:

$$h_f = f \frac{L}{d} \frac{V^2}{2g} \quad (4.3)$$

The dimensionless parameter f is the *Darcy friction factor*, which establishes a relationship between roughness and pipe resistance. ϵ is the wall roughness height, which is significant only in turbulent pipe flow. It has been shown that ϵ has orders of magnitude *less of an effect* on laminar pipe flow. An alternative form of the friction factor is

$$\frac{8\tau_w}{\rho V^2} = f = F(Re_d, \frac{\epsilon}{d}) \quad (4.4)$$

where F represents some relationship between the Reynolds Number Re_d and the average pipe roughness to diameter ratio ϵ/d (also known as relative roughness).

Piping Design Parameters		
Name	Value	Unit
Propellant	Ethyl alcohol (95%)	N/A
μ , Dynamic viscosity	0.001232	$kg/m \cdot s$
ρ , Density	789	kg/m^3
L , Pipe length	1.0	m
d , Pipe diameter	6.35	mm
\dot{m} , Mass flow rate	0.694	kg/s
Pipe material	316 stainless steel or 6061 aluminium	N/A
ϵ , Roughness	0.5 to 1.5	μm

Table 6: Design parameters and fluid properties required for pipe calculations.

Table 6 shows the piping parameters necessary for following calculations. The pipe length was estimated using a model of the test stand discussed in a later section, but is a very conservative estimate. The pipe diameter is constrained to a value of 6.35 mm (1/4 inch) due to budget constraints on the MPV, which houses a 1/4 inch port. The roughness ϵ is based on the pipe material and was extracted from engineering databases.

The behavior of turbulent and laminar flows are significantly different when considering flow characteristics of a viscous flow through a frictional pipe. Thus, it is important to determine which type of flow is expected. Using values from 6, we quickly realize our flow is most likely turbulent

$$Q = \frac{\dot{m}}{\rho} = \frac{0.694 \text{ kg/s}}{789 \text{ kg/m}^3} = 8.80 \times 10^{-4} \text{ m}^3/\text{s} \quad (4.5)$$

$$v = \frac{Q}{\pi R^2} = \frac{(8.80 \times 10^{-4} \text{ m}^3/\text{s})}{\pi[(0.00635 \text{ m})/2]^2} = 27.79 \text{ m/s} \quad (4.6)$$

$$\nu = \frac{\mu}{\rho} = \frac{0.001232 \text{ kg/m} \cdot \text{s}}{789 \text{ kg/m}^3} = 1.56 \times 10^{-6} \text{ m}^2/\text{s} \quad (4.7)$$

$$Re_d = \frac{vd}{\nu} = \frac{(27.79 \text{ m/s})(0.00635 \text{ m})}{1.56 \times 10^{-6} \text{ m}^2/\text{s}} = 113013 \quad (4.8)$$

since $Re_d \gg 2300$ (a Reynolds Number above 2300 is the accepted threshold). Though many differences are present between turbulent and laminar flow in the context of fluid flow through a pipe, perhaps the most important is that the head loss and pressure drop in turbulent flows are heavily affected by pipe roughness. In fact, there are different sets of equations applied when solving for turbulent flows, depending on the relative roughness of the pipe it is travelling through. These categories are [5]

$$\begin{aligned} \frac{\epsilon u^*}{\nu} < 5 &= \text{hydraulically smooth walls, no effect of roughness on friction} \\ 5 \leq \frac{\epsilon u^*}{\nu} \leq 70 &= \text{transitional roughness, moderate Reynolds Number effect} \\ \frac{\epsilon u^*}{\nu} > 70 &= \text{fully rough flow, sublayer broken up and friction independent of } Re \end{aligned}$$

For a smooth-walled pipe, the relation between friction factor and Reynolds Number for turbulent pipe flow is

$$\frac{1}{f^{1/2}} = 2.0 \log(Re_d f^{1/2}) - 1.8 \quad (4.9)$$

An alternate form of equation 4.9 can be used to explicitly solve for f from Re_d :

$$f = \begin{cases} 0.316 Re_d^{-1/4} \\ (1.8 \log \frac{Re_d}{6.9})^{-2} \end{cases} \quad \text{when } 4000 < Re_d < 10^5 \quad (4.10)$$

For correlating pipe friction to Reynolds Number, although for a limited range of low turbulent Reynolds Numbers, from Equation 4.10 it was was derived that

$$h_f = \frac{\Delta p}{\rho g} = f \frac{L}{d} \frac{V^2}{2g} \approx 0.316 \left(\frac{\mu}{\rho V d} \right)^{1/4} \frac{L}{d} \frac{V^2}{2g} \quad (4.11)$$

or

$$\Delta p \approx 0.158 L \rho^{3/4} \mu^{1/4} d^{-5/4} V^{7/4} \quad (4.12)$$

Substituting $Q = \frac{1}{4}\pi d^2 V$ into Equation 4.12 gives

$$\Delta p \approx 0.241 L \rho^{3/4} \mu^{1/4} d^{-4.75} Q^{1.75} \quad (4.13)$$

Equation 4.13 is critical to understanding pipe sizing. Analysing Equation 4.13 shows that for a fixed flow rate Q , the turbulent pressure drop decreases with diameter every sharply. Thus, the easiest way to reduce required pumping/upstream pressure is to increase the pipe diameter.

For fully rough flows (independent of Reynolds Number):

$$\frac{1}{f^{1/2}} = -2.0 \log \frac{\epsilon/d}{3.7} \quad (4.14)$$

To model the transitionally rough range, an general interpolation formula was created:

$$\frac{1}{f^{1/2}} = -2.0 \log \left(\frac{\epsilon/d}{3.7} + \frac{2.51}{Re_d f^{1/2}} \right) \quad (4.15)$$

Equation 4.15 is the accepted formula for determining turbulent friction. Plotting this relation gives the *Moody chart* for pipe friction (see Figure 22). Equation 4.15 is sometimes cumbersome to evaluate for f if Re_d is known, so an alternate explicit formula was developed and as

$$\frac{1}{f^{1/2}} \approx -1.8 \log \left[\frac{6.9}{Re_d} + \left(\frac{\epsilon/d}{3.7} \right)^{1.11} \right] \quad (4.16)$$

and varies less than 2 percent from Equation 4.15 [5].

The head loss and Δp values can now be computed using the Moody Chart (Figure 22) and/or Equation 4.16. Once again recalling parameters given in Table 6 and the short velocity and Reynolds number calculations given below Table 6, these values can directly be inserted into Equation 4.16 to find the friction factor f :

$$\frac{1}{f^{1/2}} \approx -1.8 \log \left[\frac{6.9}{Re_d} + \left(\frac{\epsilon/d}{3.7} \right)^{1.11} \right]$$

$$f = \left(-1.8 \log \left[\frac{6.9}{113013} + \left(\frac{(1.5 \times 10^{-6} m)/(6.35 \times 10^{-3} m)}{3.7} \right)^{1.11} \right] \right)^{-2} = 1.854 \times 10^{-2}$$

Now using Equation 4.11 we can find the head loss h_f :

$$h_f = \frac{\Delta p}{\rho g_0} = f \frac{L}{d} \frac{V^2}{2g_0}$$

$$h_f = (1.854 \times 10^{-2}) \left(\frac{2.0 m}{6.35 \times 10^{-3} m} \right) \left(\frac{(27.79 m/s)^2}{2(9.81 m/s)} \right) = 229.85 m$$

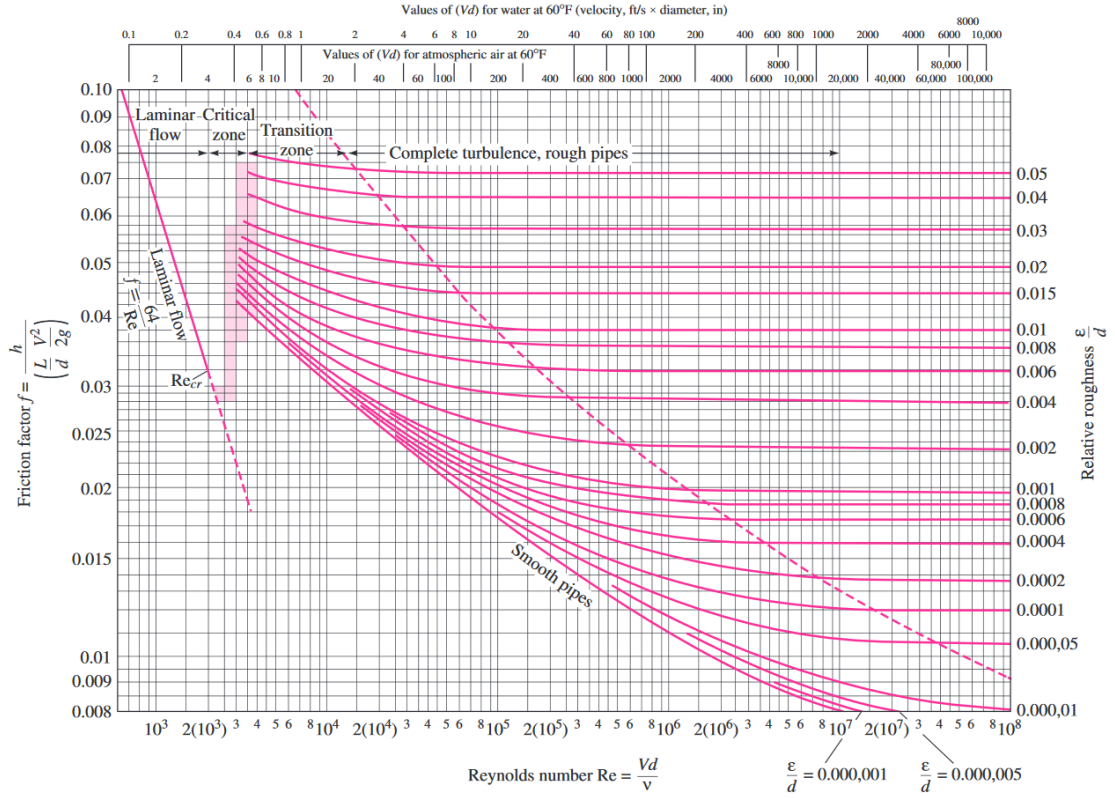


Figure 22: The Moody Chart [5]

The Δp_{ext} is therefore simply

$$\Delta p = h_f \rho g_0 = (229.85 \text{ m})(789 \text{ kg/m}^3)(9.81 \text{ m/s}^2) = 1779058 \text{ Pa} \approx 1.78 \text{ MPa}$$

This pressure drop is unacceptable. With a pressure drop purely due to head loss higher than that of chamber pressure, it is unreasonable to continue design. Typically, pressure losses due to pipe length are negligible since the higher flow rates and wider pipe diameters reduce the head loss term and flow velocity significantly. However, as mentioned previously, this design is constrained to a pipe diameter of 6.35 mm (1/4 inch) due to the MPV. Thus, since the only solution to reducing head loss is either widening or reducing the length of the pipe, the best course of action is to increase the system pipe diameter to 1/2 inch (12.7 mm) and to use a reducing adapter to accommodate the MPV. Although the reducer will produce head loss and a pressure drop of its own, it is insignificant compared to the 1.78 MPa pressure drop as expected from a universal 1/4 inch pipe system.

Figure 23 shows the effect of varying pipe diameters and pipe roughness on the expected pressure drop from head loss. It is apparent that by the exponential nature of the relationship between diameter and Δp that the best method of reducing Δp is by widening the diameter; a two-fold increase in diameter yields around a four-fold decrease in pressure drop. Although previously it was discussed that pipe roughness has a larger impact on the Δp of turbulent flow than laminar flow, it is clear from Figure 23 that this effect is still relatively small.

Using a pipe diameter d of 12.7 mm, Equations 4.16 and 4.11, and updating the fluid velocity and Reynolds Number from Equations 4.6 and 4.8, Δp_{ext} is recalculated:

$$v = \frac{Q}{\pi R^2} = \frac{(8.80 \times 10^{-4} \text{ m}^3/\text{s})}{\pi[(0.0127 \text{ m})/2]^2} = 6.947 \text{ m/s}$$

$$Re_d = \frac{vd}{\nu} = \frac{(6.947 \text{ m/s})(0.0127 \text{ m})}{1.56 \times 10^{-6} \text{ m}^2/\text{s}} = 56554$$

$$f = \left(-1.8 \log \left[\frac{6.9}{56554} + \left(\frac{(1.5 \times 10^{-6} \text{ m})/(1.27 \times 10^{-2} \text{ m})}{3.7} \right)^{1.11} \right] \right)^{-2} = 2.052 \times 10^{-2}$$

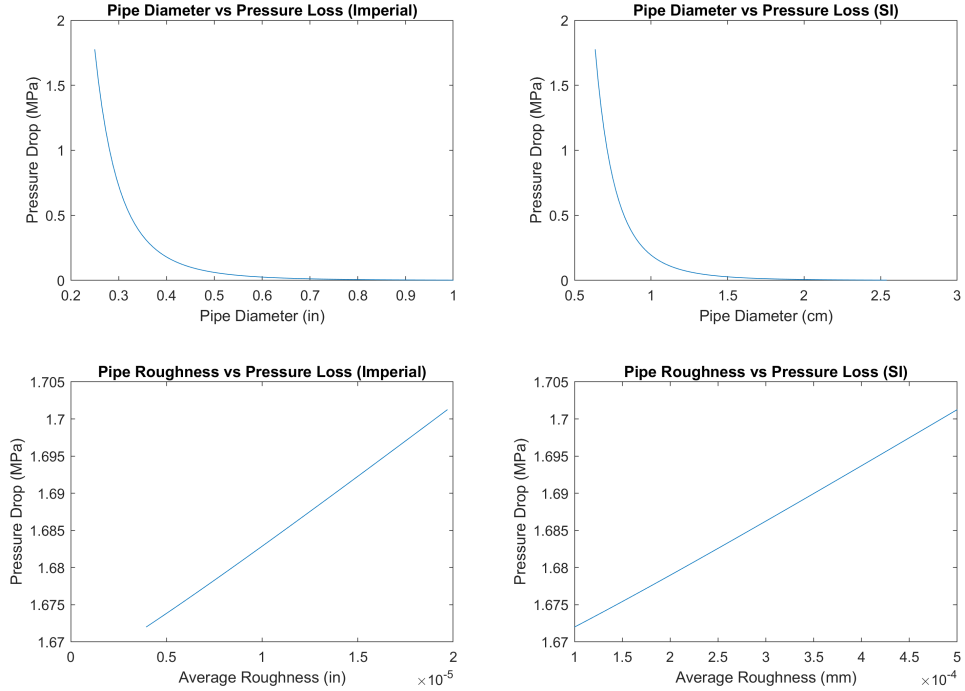


Figure 23: Pressure drops for varying pipe diameters and pipe roughness using flow parameters specified in Table 6. Both imperial and SI units are provided.

$$h_f = (2.052 \times 10^{-2}) \left(\frac{2.0 \text{ m}}{1.27 \times 10^{-2} \text{ m}} \right) \left(\frac{(6.947 \text{ m/s})^2}{2(9.81 \text{ m/s})} \right) = 7.949 \text{ m}$$

$$\Delta p = h_f \rho g_0 = (7.949 \text{ m})(789 \text{ kg/m}^3)(9.81 \text{ m/s}^2) = 61524 \text{ Pa} \approx 61.52 \text{ kPa}$$

Thus, $\Delta p_{ext} = 61.52 \text{ kPa}$ for a 1/2 inch pipe system, which is more than one order of magnitude lesser than that of a 1/4 inch pipe system.

[TABLE OF SUMMARIZED STUFF]

4.3 Tank Sizing

Another design point for pressure-fed systems involves ullage fractions. The ullage in a propellant tank is simply the percentage of tank volume that is not occupied by the propellant itself, i.e. the space that the pressurant occupies. Though complex models may be developed to more accurately model the expansion of the pressurant as the tank drains, it is commonly accepted that either the ideal gas law ($P_1 V_1 = P_2 V_2$) or an isentropic expansion model is adequate. It is apparent that due to the ideal gas law, a larger ullage is desirable since it would cause a more stable chamber pressure throughout engine operation to be observed. A literature review was conducted and showed that common practice involved a ullage fraction of around 2/3 (via Copenhagen Suborbitals and MASA). As for the nitrous tank, the process for determining a ullage fraction is nontrivial. Since the vaporization rate, along with many other dynamical aspects of nitrous behavior, is nonlinear and difficult to determine, either sufficiently complex models or reference data is required. A review of many cold-flow and hot-fire tests (especially those from participants in the Intercollegiate Rocket Engineering Competition, or IREC) was conducted, particularly examining the plots of pressure profiles for nitrous oxide. It was found, along with advisories from MASA, that the nitrous ullage should be around 5%. This will be elaborated upon in a later section, but in essence, a reasonable ullage is still required for nitrous (although it is self-pressurizing) due to its vaporization rate. It takes a moderate amount of time for the nitrous to begin boiling and repressurizing once the engine begins to run, and during this time, the propellant tank is only being pressurized by the ullage space. If the ullage percentage is low, a slight expansion in the ullage volume would represent a disproportionately large relative increase in volume as compared to its increase if it were to occur

mid-burn. Thus, this dramatic relative increase in volume causes a massive pressure drop in the opening seconds of an engine run if the initial ullage fraction is not sufficiently high.

The relation for isentropic expansion is

$$\frac{p_2}{p_1} = \left(\frac{V_1}{V_2} \right)^\gamma \quad (4.17)$$

where a subscript of 1 represents initial conditions and subscript of 2 represents final conditions. Since a burn time t_b was established in 1 to be around 5 seconds, a constant density ρ of 789 kg/m^3 and mass flow rate $dot{m}_f$ of 0.139 kg/s can be used to find that the initial volume occupied by ethanol is $[(0.139 \text{ kg/s})(5 \text{ sec})/(789 \text{ kg/m}^3)](1000 \text{ m}^3/L) = 0.881 \text{ L}$. The same procedure can be followed for nitrous and is found to be 3.59 L . Using the premeditated ullage fraction of $2/3$, it is apparent that the initial ullage volume for ethanol should be $V_1 = (0.881 \text{ L})(3)(2/3) = 1.76 \text{ L}$ and thus the total tank volume is $V_{total} = 0.881 \text{ L} + 1.76 \text{ L} = 2.64 \text{ L}$. Then, using Equation 4.17 and a γ value for N_2 gas of 1.40, an initial ethanol propellant tank pressure can be calculated:

$$p_1 = \left[\frac{p_2}{(V_1/V_2)^\gamma} \right] = \left[\frac{p_2}{(V_1/V_2)^\gamma} \right]$$

ADD TABLE OF SUMMARIZED PARAMS Engine cycle (pressure fed) Goals: measuring pressure and Cv values Divide into two sections a fluid flow velocity of less than 6 m/s to avoid water hammer effects [Zucrow Laboratories]

The plumbing system was designed with key considerations in mind which would make the system as versatile and safe as possible in the event of errors or hardware problems. The most important of these was that all pressurization and post-pressurization actions must be done remotely. Furthermore, the system must be able to vent pressure and drain propellant both remotely and manually. Finally, the system must have adequate redundancy where it is necessary to ensure safety. Figure ?? displays the full piping and instrumentation diagram for the Aphlex 1B cold flow test. The following subsections will go into detail on the different aspects of the plumbing system. It is important to note that the ethanol fill and pressurization use the same inlet in order to save costs and avoid purchasing unnecessary hardware.

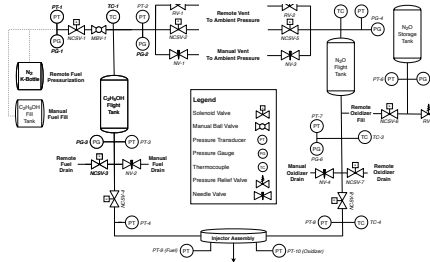


Figure 24: Full system piping and instrumentation diagram (P&ID).

4.4 Ethanol Propellant Tower Plumbing

4.4.1 Ethanol Fill System

Gravity fill was chosen for ethanol as it avoids the use of expensive or complicated pumps, making it a simple and cost-effective solution. First, ethanol will be poured manually into the tank since it is safe and not toxic, cryogenic, or at a high pressure where it might pose danger to someone manually handling it. During this time both MBV-1 and NCSV-1 will be open. Once this is complete, MBV-1 and NCSV-1 will be closed and the nitrogen K-bottle will be attached at this port to the rest of the piping system. This system is displayed in Figure 25.

4.4.2 Ethanol Nitrogen Blowdown Pressurization System

Pressure blowdown was chosen as the method of pressurization due to its simplicity along with a few other benefits. For example, in a rocket launch the utilization of pressure blowdown would allow the pressurant tank to remain on the ground (disconnection via quick disconnects and pneumatic actuators), which would significantly lower the GLOW of the rocket. Additionally, the large ullage percentage of

the propellant run tank and short engine burn time would decrease the potential benefits of a pressure-regulated system. The nitrogen for the pressure blowdown will be a K-bottle with 2,000 PSI nitrogen.

To describe procedures, NCSV-1 will be remote-operated for control of pressurant flow, while MBV-1 is the isolation valve to ensure that pressurant is not unintentionally released when engineers are near the test stand. PT-1 and PG-1 will provide data on the pressurant tank pressure. Once ethanol has been filled, the nitrogen K-bottle has been properly connected, and all other checks are completed, the nitrogen K-bottle valve will be opened and PT-1 and PG-1 will start reading pressurant pressure data. Finally, MBV-1 will be opened at this time and all personnel will leave the test stand area and return to the team's safety bunker. NCSV-1 will then be opened remotely, allowing nitrogen from the K-bottle to flow into the tank until the tank is pressurized to the proper pressure. This system is displayed in Figure 25.

Figure 25: Ethanol Fill and Nitrogen Blowdown Pressurization System

4.4.3 Ethanol Pressure Vent System

The ethanol pressure vent system consists of 3 main valves. The first of these, RV-1, a pressure relief valve, will be automatically set to open if tank pressure increases to above 600 PSI, which is about 50% greater than would be nominally expected. The second valve, NCSV-2, a solenoid valve, will be remotely opened for small pressure vents, in the case of a failure with RV-1, or a full system abort. Finally, NV-1, a needle valve, will be used for any manual draining purposes as a last and to slowly ease tank pressure once the solenoids and pressure relief valves have dumped pressure adequately enough that engineers can safely approach the test stand. This system implements redundancy (RV-1 and NCSV-2) to ensure that there is always a back-up to relieve tank pressure when it is necessary even if a valve fails. This system is displayed in Figure 26.

4.4.4 Ethanol Drain System

The ethanol system consists of two valves for drainage. The first is NCSV-3, a remotely-operated solenoid, which will be used for most draining purposes, particularly in the case of a system abort. The second valve is NV-2, a manually-operated needle valve, which will serve as a way of draining propellant manually when the tank's pressure has adequately relieved. This system is displayed in Figure 27.

4.5 Nitrous Oxide Propellant Tower

4.5.1 Nitrous Oxide Fill System

4.5.2 Nitrous Oxide Self-Pressurization System

4.5.3 Nitrous Oxide Vent System

4.5.4 Nitrous Oxide Drain System

5 Ethanol Cold Flow Test Stand Design

The ethanol cold flow test will entail running water through the full ethanol propellant tower, as well as through the injector and into the engine. The main reasons for this test include empirically verifying theoretical calculations and pressure drops, verifying system integrity, and ensuring that all



Figure 27: Ethanol Drain System

programming procedures function nominally. Most importantly, this will be the first major hardware test and will test procedures for assembly, leak-checking, filling, pressurization, draining, data-collection, valve control, and aborting.

This test will be run in two different ways: at full pressure and at scaled pressure, each of which will provide different valuable information and procedural practice to progress towards a static hot fire of the engine.

A full pressure cold flow test involves pressurizing the tank to the pressure it will be at during an actual fire, and this is to test the pressure rating of all parts of the system such as valves and sensors, and stress testing the system to verify performance levels. Furthermore this can be used to ensure that this system can safely operate at its normal working pressure, including whether pressure can be properly relieved in the case of an abort.

Scaled pressure, however, is making the pressure differential between the tank and chamber equal to the actual differential we will be expecting in the static fire. Since there will be no combustion in the chamber, its pressure will be at 1 atm. This is much lower than the actual combustion chamber temperature and would therefore result in a higher mass flow rate if our tank pressure remained the same. By properly scaling down our tank pressure, it would be possible to accurately measure the system Cv, as well as to determine mass flow rate and tank pressure depletion profile over time.

To accomplish these goals, the plumbing detailed in section 4.1 must be fully constructed as a test stand, along with a separate injector and engine mechanism which could later be used to measure thrust in an actual static fire. The following subsections will detail these two major parts of the test stand for this test.

5.1 Tank Stand and Plumbing

The tank stand and plumbing had to contain the ethanol flight tank, nitrogen K-bottle for pressurization, and all the plumbing up until the engine. The design for this test stand included a frame of aluminum 80/20s which would hold the ethanol flight tank in place, as well as cinder blocks as a stand for the temporary nitrogen K-bottle. The plumbing will mostly be bolted to a 1/8" thick steel plate on the outside of the 80/20 steel frame for the ethanol tank. The use of plate will allow for all plumbing to be visible and easily accessible for small changes or for turning manual valves, as well as for pressure gauges to be monitored via video camera live stream in the event of a pressure transducer failure. The

plate will additionally serve as a support structure for the piping. A rendering of the ethanol tower tank stand and plumbing section is shown in Figure 28.



Figure 28: Ethanol Propellant Tower Test Stand Render

Both plates of plumbing were designed according to the designed piping and instrumentation diagram in Figure ???. When designed in 3D space, they were made to be as compact as possible to reduce total material needed. Pressure relief valves were also designed to point away from any other mounted instrumentation. All major components including valves, joints, gauges, sensors, and AN to NPT adaptors were included in the rendering. Renderings of the upper and lower plates of plumbing are shown in Figures 29 and 30 respectively.

Because the nitrogen K-bottle has to be connected to the plumbing from a tube located at the top of the upper plate, the cinder block arrangement was used to elevate the K-bottle, reducing the amount of tubing needed to reach that location. This method of reducing external tubing was determined to be easier and more efficient than other methods such as fulling mounting the K-bottle above the upper plumbing plate, which would have been difficult due to the extra support needed to handle that weight. Additionally, the availability, ease of construction, and flexibility of arrangement for the cinder blocks made them an appealing choice. A full system render of the ethanol stand, plumbing, and K-bottle is shown in Figure 31.

5.2 Engine and Injector

6 Parts and Budget

6.1 Valves

Valve Type	Max Pressure	Cv	Manufacturer	Part Number
Solenoid	1200 psi	0.7	Holley/NOS	18070NOS
Pressure Relief	1000 psi	???	Generant/Rego	VRVH-250-B-B-600
Full-Port Ball	1000 psi	16	DiscoverValve	101097
Needle	5000 psi	0-0.4	Generant	3000-4-B



Figure 29: Upper Plate Render



Figure 30: Lower Plate Render



Figure 31: Ethanol Propellant Tower Test Stand with Nitrogen K Bottle Render

6.2 Sensors

Sensor Type	Max Pressure	Outlet	Manufacturer	Part Number
Pressure Gauge	1000 psi	1/4" MNPT	UPE Group	N/A
Pressure Transducer	1000 psi	1/8" MNPT	Ebay	N/A
Thermocouple	???	1/4" MNPT	Omega	N/A

6.3 Fittings

Fitting Type	Manufacturer	Part Number
T-Joint	Jegs	N/A
Cross-Joint	Jegs	N/A
1/4" AN to 1/2" NPT	Jegs	N/A
1/4" AN to 1/4" NPT	Jegs	N/A
1/4" AN to 1/8" NPT	Jegs	N/A

6.4 Tools

Tool	Manufacturer	Part Number
Tube Cutter	Ridgid	N/A
Tube Deburrer	Ridgid	N/A
Tube Bender	Imperial	N/A
Tube Flarer	Ridgid	N/A
Tube Straightener	???	N/A

6.5 Other Parts

Part	Max Pressure	Function	Manufacturer	Info	Part Number
Nitrogen	N/A	Pressurization	Praxair	Rental	N/A
Regulator	???	Pressure Regulation	???	???	N/A
Tubing	1200 psi	N/A	McMaster	6ft unit, 0.01" thick	N/A
Stainless Steel	42000 psi	Injector Material	???	???	N/A

6.6 Budget

Part	Quantity	Unit Cost	Total Cost
Solenoid Valve	4	271.95	1087.80
Pressure Relief Valve	1	34.30	34.30
Ball Valve	1	10.79	11.40
Needle Valve	2	22.50	45.00
Pressure Gauge	3	14.50	43.50
Pressure Transducer	4	20.00	80.00
Thermocouple	1	00.00	00.00
Load Cell	1	00.00	00.00
T-Joint	7	11.60	81.20
1/4" AN to 1/2" NPT	5	10.49	52.45
1/4" AN to 1/4" NPT	9	3.60	32.40
1/4" AN to 1/8" NPT	0	3.60	00.00
Tube Cutter	1	37.73	37.73
Tube Deburrer	1	37.95	37.95
Tube Bender	1	45.00	45.00
Tube Flarer	1	145.00	145.00
Tube Straightener	1	128.00	128.00
Nitrogen	1	20.00	20.00
Regulator	1	100.00	100.00
Tubing	5	38.25	191.25
Stainless Steel	1	25.00	25.00
Total	N/A	N/A	2,172.98

References

- [1] Tomasz Palacz. "Nitrous Oxide Application for Low-Thrust and Low-Cost Liquid Rocket Engine". In: *7th European Conference for Aeronautics and Space Sciences* (July 2017).

- [2] GVR Rao. "Exhaust Nozzle Contour for Optimum Thrust". In: *Jet Propulsion Archive* 28.6 (June 1958).
- [3] George P. Sutton and Oscar Biblarz. *Rocket Propulsion Elements, 9th Edition*. Wiley, Dec. 2016.
- [4] Travis S. Taylor. *Introduction to Rocket Science and Engineering*. CRC Press, 2009.
- [5] Frank M. White. *Fluid Mechanics*. Fourth. McGraw-Hill Series in Mechanical Engineering. McGraw-Hill, Dec. 1998.